Phys. Status Solidi B **247**, No. 7, 1600–1607 (2010) / **DOI** 10.1002/pssb.200945417

physica status solidi b
www.pss-b.com
basic solid state physics

Feature Article

Ab initio study of magnetoelectricity in composite multiferroics

M. Fechner*[,1], I. V. Maznichenko[2], S. Ostanin[1], A. Ernst[1], J. Henk[1], and I. Mertig[1,2]

[1] Max-Planck-Institut für Mikrostrukturphysik, Weinberg 2, 06120 Halle, Germany
[2] Institut für Physik, Martin-Luther-Universität Halle-Wittenberg, 06099 Halle, Germany

Received 7 September 2009, revised 4 January 2010, accepted 27 January 2010
Published online 26 March 2010

Keywords magnetoelectric effects, multiferroics

* Corresponding author: e-mail fechner@mpi-halle.de

The coexistence of magnetism and ferroelectricity in the same crystalline phase of a so-called multiferroic (MF) material involves the opportunity of magnetoelectric (ME) coupling. ME coupling, in principle, offers magnetization switching by an electric field or polarization switching by a magnetic field. Since this phenomenon allows to store information in nanometer-sized memories with four logic states, the issues of MFs are of prime interest. In the single-phase MFs, however, the electric polarization and magnetization interact weakly with each other while ferromagnetism disappears far below room temperature. A more robust scenario of magnetoelectricity might occur in artificial MFs composed of ferromagnetic (FM) thin films which are grown epitaxially on a ferroelectric substrate. In the study of composite MFs, the results of *ab initio* calculations have shown an extremely promising direction for the next years. Although these calculations go ahead of experiment they explore the trends and basic physics of ME. Here, on the basis of first-principles calculations we predict that epitaxial ultrathin Fe films deposited on TiO_2-terminated (001) surface of $ATiO_3$ perovskites (A = Pb, Ba) exhibit an unexpected change in their magnetic structure with increasing Fe-film thickness. The magnetic order changes from strongly FM for the single-monolayer Fe system to ferrimagnetic with almost vanishing magnetization upon deposition of a second Fe layer. FM order is restored for thicker Fe films. This effect can be understood in terms of hybridization of electronic states and structural relaxation. Additionally, we study the effect of iron oxidation on the ME coupling at the $Fe_2/ATiO_3(001)$ interface. The oxygen coverage ranged between 0.5 and 2.0 adsorbed O atom per Fe atom. The magnetic properties of the Fe layer are gradually degraded with increasing O coverage. However, the change in magnetization which is induced by the electric polarization reversal remains robust for all energetically favorable compositions. Thus, the surface oxidation of composite MFs cannot destroy the switchable magnetoelectricity.

1 Introduction to composite multiferroics When any two of all four primary ferroic properties, i.e., ferroelectricity, ferromagnetism, ferroelasticity, and ferrotoroidicity coexist in a so-called multiferroic (MF) material [1], its symmetry must be restricted dramatically [2]. In the absence of space-inversion and time-reversal symmetry, the occurrence of ferroelectricity and magnetism in the same phase of an MF allows the observation of both a switchable electric polarization, P, and a switchable magnetization, M, sketched in Fig. 1. In principle, this phenomenon allows to store information in nanometer-sized memories with four logic states [3–5].

Although some single-phase MFs, such as $BiFeO_3$ and $RMnO_3$ (R rare earths), were studied since the 1970s [6], the search for novel MFs is not finished yet. [7]. Moreover, their classification, which is based on the different mechanisms of induced polarity, has been revised since 2003 (see Ref. [8] and references therein)when the type-II class of magnetic MF was established. The type-I class of MFs contains numerous perovskite-like materials in which ferroelectricity and magnetism appear independently of one another and where P appears at higher temperatures than magnetism. One can find several subclasses of type-I MF, depending on the mechanism of their ferroelectricity [8]. In a type-II MF, ferroelectricity is driven by the electronic order degrees related to spin arrangements which break inversion symmetry. This symmetry breaking occurs due to a spin–orbit-related mechanism in conjunction mostly with the spin-spiral magnetic structure. For instance, this happens in $TbMnO_3$ below 28 K when the Mn spin tips sweep out a

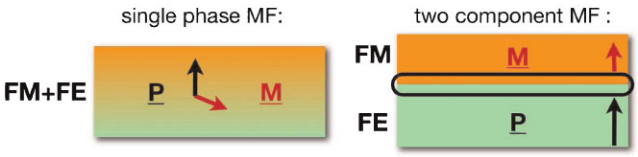

Figure 1 (online color at: www.pss-b.com) Single-phase and composite MFs are sketched in the left and right panels, respectively. In the single-phase MF, its magnetoelectricity is the volume effect while for composite MF, in contrary, the ME coupling is confined to the interface area.

cycloid. Such cycloidal spin arrangement via the Dzyaloshinskii–Moria antisymmetric exchange creates a polarization: $P \sim \boldsymbol{r}_{ij} \times [S_i \times S_j]$, where $\boldsymbol{r}_{ij}$ is the vector connecting neighboring spins S_i and S_j. There is another subclass of the type-II MFs where ferroelectricity may appear for some collinear antiferromagnetic structures below the Néel temperature due to the Heisenberg-like symmetric exchange. Thus, ferroelectricity of the type-II MF is caused by a particular type of magnetic order, which exists only at low temperature and which is predominantly antiferromagnetic.

In MF, an applied electric field, E, displacing the magnetic ions, affects the magnetic exchange coupling or, vice versa, the external magnetic field, H, induces the electric polarization: $P_i \sim \alpha_{ij} H_j$, where α_{ij} is the magnetoelectric (ME) tensor and $(i,j) = x, y, z$. According to the Landau theory, the linear ME [1] contribution to the Gibbs-free energy is $\alpha_{ij} E_i H_j$. If α is sufficiently strong then M can be easily modified by E. It should be kept in mind that magnetoelectricity is a bulk intrinsic property for which the induction of M depends linearly on E. In the type-I single-phase MF, P and M weakly interact with each other and, therefore, α is marginal there. Besides, all these MFs possess a hierarchy of phase transformations [9], where the magnetism disappears far below room temperature. In a type-II MF, the magnitude of P is never large. However, these materials disclose a relatively large ME coupling. For instance, the direction of P in $TbMnO_3$ may flop by 90° when an applied magnetic field forces the plane of a magnetic cycloid to rotate by 90°. Obviously, the quest for fundamentally new MFs requires a better understanding of the mechanisms which mediate the ME coupling.

Studies based on density-functional theory (DFT) have significantly contributed to this rapidly developing field of single-phase MFs [10]. Although these calculations go ahead of experiment they explore the trends and basic physics of ME. For instance, *ab initio* calculations predict that a voltage of about 30 meV, applied across a $SrRuO_3/SrTiO_3$ interface, without magnetic cations, can induce a net magnetic moment [11]. Since the space-inversion symmetry is broken between the two unlike terminations, the ME effect results entirely from spin accumulation at the interface. The effect might be enhanced by the use of materials with higher spin polarization. Indeed, a more robust scenario of magnetoelectricity occurs in epitaxially grown two-phase MF consisting of ferroelectric and ferromagnetic (FM) components. The ME effect is mediated by strain across the biferroic interface. Inaccessible by conventional synthesis, the MF composites exhibit specific properties which are superior to those of customary materials. *Ab initio* studies suggest that the interface bonding is the source of strong ME coupling in $Fe/BaTiO_3(001)$ [12, 13]. The interfacial Ti atoms show an induced magnetic moment of about $0.3\mu_B$. Moreover, for the two opposite directions of P ($P_\downarrow$ and $P_\uparrow$), there are rather noticeable differences of $0.1–0.2\mu_B$ in the magnetic moments of Fe and Ti at the interface. This is a very promising phenomenon, which is entirely confined to the ferroelectric/FM interface and which differs from the volume ME effect. The interface ME effect defines the change in magnetization at the coercive field E_c: $\mu_0 \Delta M \approx \alpha E_c$. α of about 2×10^{-10} G cm^2/V estimated for $Fe/BaTiO_3(001)$ from first principles, is two orders of magnitude larger than that predicted for $SrRuO_3/SrTiO_3$.

Epitaxial growth of the two-phase MF thin films of high quality continues to be very challenging. A 30 nm thick Fe(001) film has been grown recently on a ferroelectric $BaTiO_3(001)$ substrate [14]. For this MF, the interface FM resonance mode is characterized by a large out-of-plane magnetic anisotropy comparable to and of opposite in sign to the shape anisotropy, the latter favoring an in-plane easy axis for thick film interiors. The trends of magnetic anisotropy detected for $Fe/BaTiO_3$ (BTO) are in a good agreement with corresponding *ab initio* calculations [13, 15]. In the case of one Fe monolayer (ML), DFT predicts that perpendicular anisotropy is favored to in-plane anisotropy by 0.72 meV (0.54 meV) per Fe atom for $P_\downarrow$ ($P_\uparrow$) [13]. Although the spin-reorientation transition under switching of P is not found from first principles, the ME coupling alters the magnetocrystalline anisotropy energy by about 50%. The magnetic order of $Fe/BaTiO_3$ can be tuned by the Fe layer thickness to ferrimagnetic with almost zero M upon deposition of a second Fe ML [13]. FM order is restored for Fe films thicker than 3 ML, for which the shape anisotropy energy favors in-plane alignment of M [15].

Recently, Niranjan et al. [16] modeling different $Fe_3O_4/BaTiO_3(001)$ interfaces within DFT, have found that ME coupling is stronger for the O-deficient type of the Fe_3O_4 interface. This suggests that the presence of oxygen or oxygen vacancies at the biferroic interface plays an important role. The temperature-dependent magnetization curves of epitaxial magnetite films grown on $BaTiO_3(001)$ demonstrate [17] a strong perpendicular magnetic anisotropy, which is modified by the piezoelectric response of the substrate. Figure 2 illustrates the two experimental setups for the interface ME coupling.

2 Magnetoelectric coupling in $Fe/ATiO_3$ (A = Ba, Pb) In the following we give a detailed example of the ME coupling at an interface and we present results obtained from first principles [13]. A perfect model system for an MF interface is an $ATiO_3$ (A = Ba or Pb) substrate covered with few iron layers (Fig. 3). Both materials are not only ferroic separately at room temperature but also as a two-

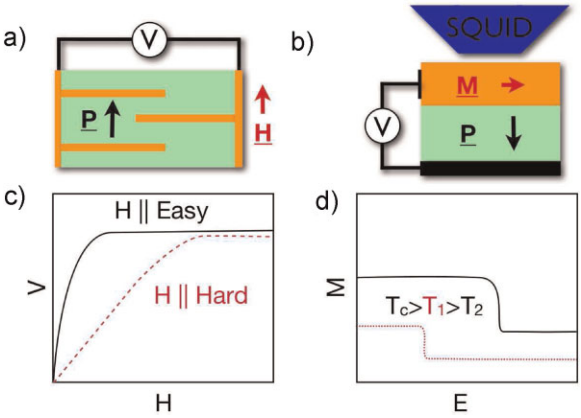

Figure 2 (online color at: www.pss-b.com) The schemes (a) and (b) in the upper panels show experimental setups for determining the ME coupling at biferroic interfaces. The figures below (c) and (d) sketch the corresponding results of the measurements. In (a) Ni contacts are embedded in a $BaTiO_3$ matrix and an applied magnetic field gives rise to the voltage change. In (b) a $La_{1/3}Sr_{2/3}MnO$ film is deposited on top of $BaTiO_3$. SQUID allows the detection of the film magnetization under an applied bias. A detailed discussion of both experiments is given in Refs. [3, 18].

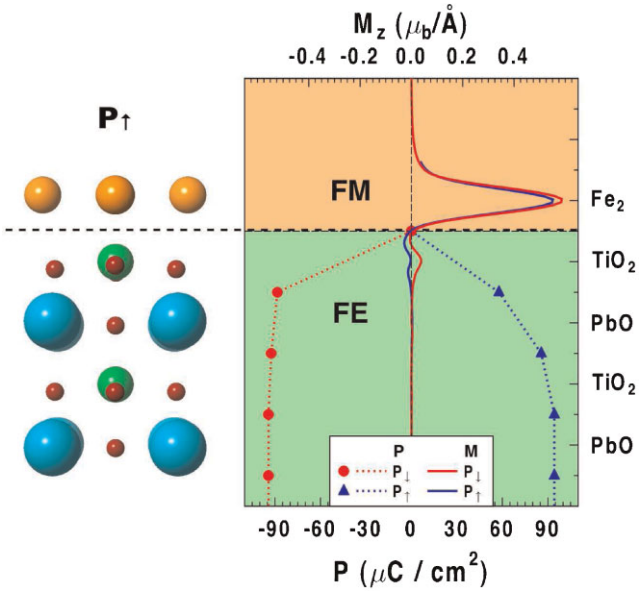

Figure 3 (online color at: www.pss-b.com) The unit cell of biferroic $Fe_2/TiO_2/ATiO_3(001)$ (A = Ba, Pb) with a 2 nm thick vacuum layer is sketched as a side view. On the right-hand side the ferroic order parameters at the interface for 1 ML Fe on top of PTO are shown. The layer resolved polarization is plotted as a dotted line, whereas the magnetization is represented by a solid line. The two colors correspond to the states $P_\uparrow$ (blue) and $P_\downarrow$ (red). The largest change of the magnetization density was obtained within the TiO_2 plane next to the interface.

component compound. The spontaneous polarization of the substrates ranges from 26 $\mu C/cm^2$ for BTO to 75 $\mu C/cm^2$ for PTO; iron has a magnetic moment of $2.25\mu_B$. More importantly, the body-centered cubic Fe and ATO(001) (A = Ba, Pb) have a good match of their in-plane lattice constant when the bcc-Fe [110] axis is aligned to the [100] axis of ATO. The mismatch of $<3\%$ allows epitaxial growth, as has recently been demonstrated for $BaTiO_3$/Fe [14].

To treat the interplay between geometric, electronic, and magnetic properties in an appropriate way we use a multicode approach. The geometric relaxations and magnetic properties are obtained by the Vienna Ab-initio Simulation Package (VASP) [19]. A cross-check of the magnetic structure obtained by VASP was done using the scalar-relativistic Korringa–Kohn–Rostoker (KKR) [20] method; the magnetocrystalline anisotropy was additionally computed with a relativistic layer-KKR code [21]. In all calculations the local spin-density approximation (LSDA) to DFT is used. Further various quantities were carefully compared among the three DFT codes to obtain consistent results. Reliability is achieved by numerous convergence tests.

At the atomic scale both materials are combined via the Fe/TiO_2 interface. The TiO_2 termination of the FE substrate was chosen since it is energetically preferable [22]. The same arguments hold for the positions of the Fe atoms which prefer to sit above the oxygen atoms. To model the reversal of the polarization direction the structural properties of the FE substrate have to be considered. Within the tetragonal phase the electric polarization in $ATiO_3$ is caused by the displacement of the atoms along the [001] axis. It can be defined as $\delta \equiv z(\text{cation}) - z(\text{O})$. For the considered systems there exist two distinguished scenarios for the atomic displacements. If the displacement in the FE substrate is positive the polarization points toward the interface; if it is negative, the polarization points away from the interface. Both situations mimic the state after polarization switching, that is in remanence. We denote the two states corresponding their polarization directions as $P_\uparrow$ and $P_\downarrow$. For our calculation they are modeled by considering the two different supercells. Each supercell consist of 5 unit cells of $ATiO_3$ (A = Ba or Pb) covered with L ML of iron and separated by 2 nm of vacuum. They differ in δ, which was set to the positive bulk value for the $P_\uparrow$ state and negative for $P_\downarrow$. The structural relaxation concerns the three top layers of the $ATiO_3$ and the Fe layer until the forces are less than 5 meV/Å.

The magnetic and ferroelectric properties are shown in Fig. 3. On the left-hand side of Fig. 3 the unit cell of $Fe_2/TiO_2/PbTiO_3(001)$ with $P_\uparrow$ is shown. For the distance between the TiO_2 and Fe at the interface we obtained – after structural relaxation independently on the iron thickness and polarization direction – a value of $a \approx 1.8$ Å. Further compression of the surface area of $ATiO_3$, which could suppress ferroelectricity, was not found. The only structural detail which is sensitive to the number of iron layers is the distance between the first and the second iron layer. In case of two layers (not shown in the figure) this distance is about 1.05 Å whereas for thicker layers it is about 1.2 Å. Later we will explain the change in the magnetic ordering caused by the structural relaxation. A detailed overview of the structure is given in Ref. [13].

At the right-hand side of Fig. 3 the two-order parameters at the interface of $Fe_2/TiO_2/PbTiO_3(001)$ are shown. The unit-cell resolved polarizations were calculated by $P_i = \delta q_{\mathrm{Born}}$, where q_{Born} is the Born effective charge. At first glance, it is clearly visible that the largest interference of the two ferroic properties is found in the TiO_2 layer. In particular the magnetization changes the sign when the polarization is turned. A change of the polarization due to the vicinity of the iron was not observed. Similarly the iron moments are only mildly influenced by the change of the polarization direction. The total change of magnetization $\Delta M = M(P_\downarrow) - M(P_\uparrow)$ for this system is about $1\mu_B$. This change will be explained by a detailed analysis of the hybridization of Fe, Ti, and O atoms at the interface in the following section.

For all substrates and Fe-film thicknesses, total energies of two magnetic configurations were computed: FM and AFM (antiferrimagnetic) ordering was considered. The left panel in Fig. 4 shows the energy difference $\Delta E = E_{\mathrm{AFM}} - E_{\mathrm{FM}}$ between these two configurations. For both substrates we obtained for 1 ML Fe FM order of the iron independently of the polarization direction. Adding a second layer changes the ordering substantially. Here, an antiferromagnetic ordering seems to be preferred. The constrained self-consistent calculations, however, did not converge toward a complete AFM configuration; forcing the top layer to be antiferromagnetic the layer beneath always shows FM order with suppressed moments. Consequently the preferred magnetic order for $L = 2$ is AFM. Deposition of a third Fe layer restores the FM order. In almost all cases, the relation of $E_{\mathrm{FM}} < E_{\mathrm{AFM}}$ is obtained. An exception is $L = 2$ for which it was not possible to reach an antiferromagnetic solution but an AFM instead. Thus, the magnetic order of the two-phase MFs can be tuned by the Fe-film thickness. Strain and electric polarizability are of minor importance for the Fe-film magnetism.

The middle panel of Fig. 4 shows the magnetization of the interface as a function of the iron layer thickness. The magnetization is normalized to the number of iron atoms to allow comparison of the results. The two curves within the figures correspond to the two polarization states, and their difference is the change of magnetization under polarization reversal. For 1 ML iron on PTO there exists a large magnetization which is mainly carried by the magnetic moments of iron $m_{\mathrm{Fe}} \approx 3\mu_B$. A difference of about $1\mu_B$ between the two polarization directions is obvious in the case of Fe on PTO. This is in contrast to the BTO substrate where this difference is tiny ($\Delta M = 0.05\mu_B$). With two layers of iron the magnetization drops down to almost zero due to the change of the above-mentioned magnetic order. Further, the two curves lie on top of each other. Upon adding more layers FM order is stabilized and the magnetization increases. For more layers the magnetization converges toward the bulk value of iron (dashed line).

Based on the change of the magnetization the surface ME coefficient is calculated. It is defined as $\alpha_{\mathrm{surf}} = \Delta M/(E_c A)$, where A is the surface area and E_c is the coercive field needed to switch the polarization. Using the experimental values of E_c for BTO (10 kV/cm) and PTO (33 kV/cm), the coupling coefficients were calculated and plotted as a function of the

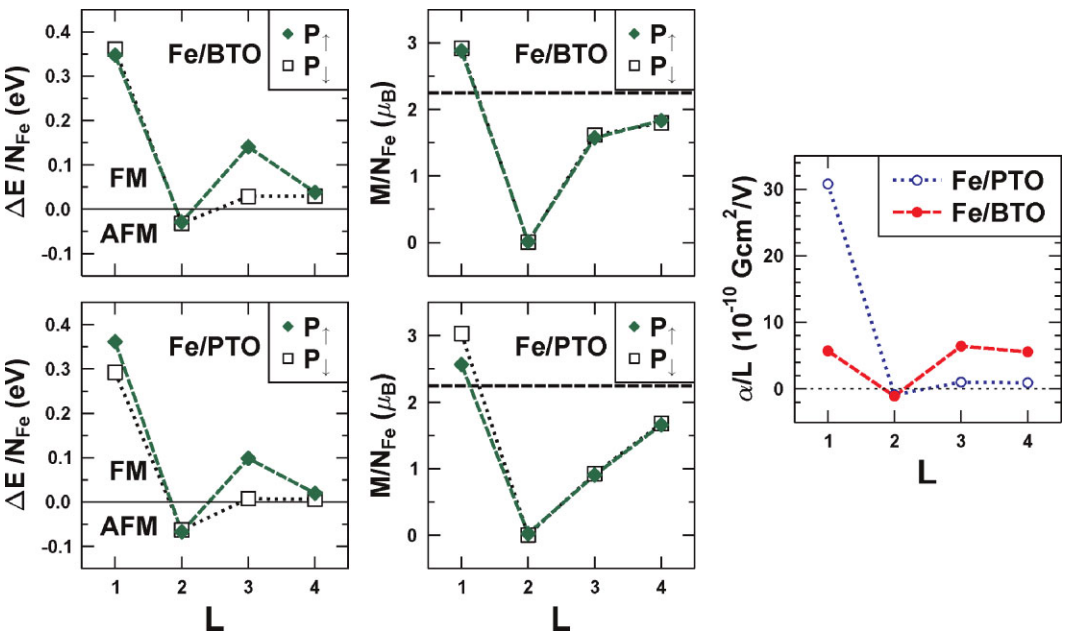

Figure 4 (online color at: www.pss-b.com) Magnetism of $(Fe_2)_L/ATiO_3(001)$ for $PbTiO_3$ (PTO) and $BaTiO_3$ (BTO) *versus* Fe-film thickness L. In the two left panels, the total-energy difference $\Delta E \equiv E_{\mathrm{AFM}} - E_{\mathrm{FM}}$ of the AFM and FM configurations are normalized with respect to the number N_{Fe} of Fe atoms in the film unit cell. In the two middle panels, the magnetization per Fe atom for the lowest-energy configuration is plotted. Here, the dashed line indicates the magnetic moment of Fe bulk. The ME coupling coefficient α of $(Fe_2)_L/ATO(001)$ (A = Ba, Pb) is plotted *versus* the Fe-film thickness L in the right panel.

number of iron layers in the right panel of Fig. 4. Since the ΔM is largest for Fe on PTO, the largest coupling is obtained for this system. Interestingly the coefficient for PTO decays with increasing number of iron layers. This is in contrast to BTO where α_{surf} stays nearly constant. An exception is the case $L = 2$ for which the value approaches zero for both substrates. Theoretical studies of superlattices of BTO and Fe show that the value for 3 and 4 layers are also valid for thick Fe films [12]. To compare these values we consider values obtained for a $SrRuO_3/SrTiO_3$ interface. *Ab initio* calculations based on the DFT predict that a voltage of about 30 meV, applied across the interface without magnetic cations, can induce a net magnetic moment [11]. This leads to an α_{surf} two orders of magnitude smaller than that predicted for the Fe/PTO system.

2.1 Microscopic origin of ME coupling From the preceding it is evident that the magnetic moments of the Fe film are changed in a complex manner by the interface. To achieve insight into the mechanism, we illustrate in Fig. 5 the spin-polarized electronic properties at the Fe/BTO interface. A switching effect is mainly seen for the minority electrons around the Fermi energy. This effect is much more obvious in the difference between the two densities for the two polarizations. The effect is clearly dominating for minority electrons whereas there are only minor changes for majority electrons. This could be attributed to a hybridization of the Fe d-minority states with the Ti d-states which leads to an induced moment on the Ti site oriented opposite to the iron moments. Since the Ti atom is closer to the Fe atoms in the $P_\uparrow$ state the hybridization is stronger for this configuration. Consequently the induced Ti moment is larger. For $P_\downarrow$ the opposite is the case and a smaller Ti moment can be observed. It turns out that in this moment which causes the difference of the total magnetization between the two polarization states.

Because of the larger displacement of the atoms this effect is even more pronounced in Fe/PTO (see the right-hand side of Fig. 3). In contrast to BTO an additional large induced moment on the oxygen could be observed in the $P_\downarrow$ case. The O moment is aligned parallel with the iron moments. Switching to $P_\uparrow$ causes an induced moment on Ti

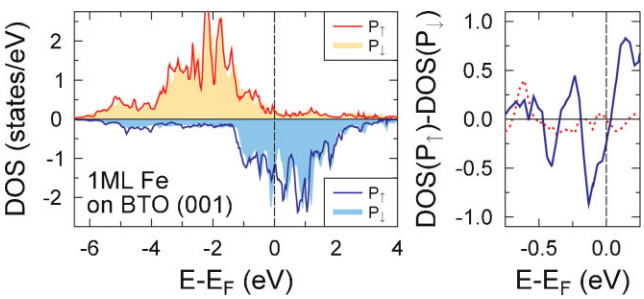

Figure 5 (online color at: www.pss-b.com) Electronic structure at the surface of $(Fe_2)_1/BaTiO_3(001)$. The left panel shows the spin-resolved density of states (DOS) for Fe/BTO. The right panel gives the difference between the spin-resolved DOS for $P_\uparrow$ and $P_\downarrow$ close to the Fermi energy E_F (majority: red, dotted; minority: blue, solid).

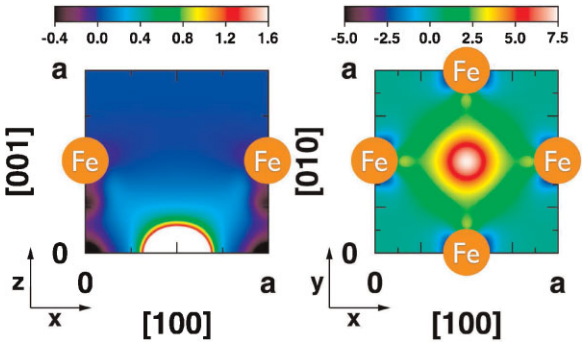

Figure 6 (online color at: www.pss-b.com) Charge redistribution of minority-spin electrons at the interface of $(Fe_2)_1/BTO(001)$ upon reversal of the electric polarization P with respect to the surface normal. The difference of the charge densities for $P_\uparrow$ and $P_\downarrow$ is depicted in a perpendicular (left) and an in-plane cut through the Fe atoms (a is the BTO lattice constant; color scales in arbitrary units). The Fe atoms are represented by spheres.

antiparallel to the iron moments which then induces a moment on the lower oxygen. The larger displacement and the additionally induced moment causes the sizable change of $1\mu_B$.

The change of the minority charge distribution in real space is shown in Fig. 6 for Fe on BTO. Considering the right-hand-side panel, it is obvious that most of the minority charge is pushed into the interstitial region between the iron atoms under polarization switching. This charge originates mainly from the Ti atom, as is evident from the side view, and is responsible for the change of magnetization under switching.

While the magnetic moments do not change sign upon P reversal, we consider the possibility of a spin-reorientation transition as another type of ME switching. To investigate this mechanism we were using the relativistic layer (KKR), the magnetic anisotropy for $(Fe_2)_1/BTO(001)$ is computed within the framework of the magnetic force theorem [23]. For both P orientations perpendicular anisotropy is favored with respect to in-plane anisotropy, namely by 0.72 meV ($P_\downarrow$) and 0.54 meV ($P_\uparrow$) per Fe atom. It is worth mentioning that the anisotropy energies are twice as large as in FePt [24, 25]. In summary we find a change in the magnetization upon polarization reversal but no alteration of the magnetization direction.

2.2 Magnetic order As previously mentioned, the magnetic order changes as a function of the Fe-layer thickness. In particular the magnetic order of two Fe layers becomes AFM (Fig. 4). For two layers the magnetic moments in the Fe interface layer are almost quenched while the sizable moments in the surface layer are ordered antiparallely. This is due to the small distance of 1 Å between the iron layers. Since the two Fe sites in the top layer are inequivalent, e.g., Fe is on top of Ti (Ba) sites. They carry different magnetic moments; this reflects the environment of these atoms, in particular the atomic volumes and the

hybridization. Polarization reversal affects mainly the positions of Ti atoms and consequently those of the Fe atoms atop. The small volume of interfacial Fe is reduced even further and leads to very small magnetic moments. The small size of Fe atoms in the interface layer explains as well the antiferromagnetic ordering of their local magnetic moments [26]. Adding a third Fe layer increases both the coordination numbers and the atomic volumes and consequently restores FM order.

2.3 Oxygen coverage So far, our *ab initio* studies of MF composites were focused on perfect interfaces without oxidants. However, the strength of the ME coupling may be sensitive to the degree of oxidation. The Fe oxidation is unavoidably motivated, firstly, by the growth process of the ferroelectric since oxygen will react with the iron during Fe growth. Secondly, for the uncovered Fe films further oxidation occurs when the sample is removed from the chamber. These two possible scenarios may result in some particular Fe–O compositions which vary from highly oxidized Fe to an almost clean surface. Thus, the *ab initio*-based modeling would be extremely useful. In the following, we study from first principles the key electronic, magnetic, and structural factors behind the oxidation process of the 1 ML Fe grown on $BaTiO_3(001)$ and $PbTiO_3(001)$. We demonstrate in which positions oxygen adatoms sit above the Fe layer and that the ME coupling in these composites is robust against the O composition [27].

The equilibrium bond length calculated for molecular O_2 is 1.23 Å. For $Fe_2/TiO_2/ATiO_3(001)$, the in-plane lattice parameter is about 3.9 Å, while the Fe–Fe separation is about 2.75 Å. The latter is two times larger than that of the O_2 dissociation. Therefore, to model the Fe oxidation of Fe/BTO and Fe/PTO we must consider O coverages, $c(O_x : Fe_2)$, ranging between $c = 1/2$ and two adsorbed O atoms per Fe atom ($c = 2$). There are 12 possible configurations for these coverages (Fig. 7). For $c = 0.5$, one oxygen adatom per unit cell can occupy the site either above A or above Ti, or alternatively atop Fe. For $c = 1$, the two O adatoms form four configurations marked in Fig. 7 as AT, AF, TF, and FF. In the case of $c = 1.5$, we relax the ATF, TFF, and AFF configurations. And, finally, for $c = 2$ there are two more possibilities to distribute four adatoms, such as ATFF (the case of full coverage) and 4H, which means that all four hollow sites are occupied by O. Using a $10 \times 10 \times 6$ Monkhorst–Pack [28] mesh for the Brillouin-zone integration, we relaxed the O adatoms and Fe atoms plus all atoms of the two top ABO_3 unit cells until the forces were less than 1.0×10^{-2} eV/Å. After relaxation, oxygen forms an overlayer above the Fe layer, with the distance depending on coverage and direction of P.

In the case $c = 0.5$, the most favorable configuration is A. However, the configurations A and T can coexist for this O coverage since the difference in energy between them is $E_T - E_A \sim 0.2$ eV. For the ABO_3 substrates, the energetics are almost the same while the P reversal yields the energy differences compatible with that of $E_T - E_A$. When

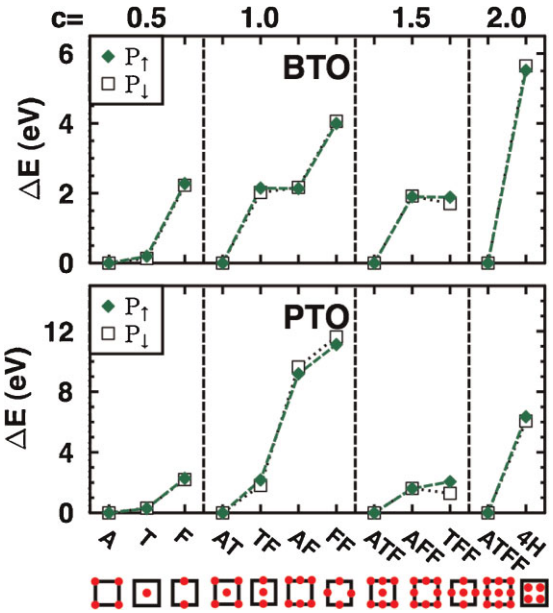

Figure 7 (online color at: www.pss-b.com) Relaxed total energy of $O_x/Fe_2/ATO(001)$ (A = Ba (top panel), Pb (lower panel), and $0 < x < 4$) is plotted for 12 simulated O configurations. The latter are given schematically below the labels. For each coverage $c = x/2$, the lowest-energy configuration pins the energy zero.

the O atom relaxes above Fe this results in the highly unfavorable configuration F, with the energy of 2.1 eV larger than that of case A. This can be understood by inspecting the relaxed structures of the A and T configurations. These are very similar to that of an O/Fe(001), which were under debate in the literature [29]; the O adatom is relaxed at the hollow site by about 0.3 Å above the Fe ML. The configurations A and T do not differ significantly with respect to each other and with respect to the uncovered 1 ML Fe on ABO_3. In the case of configuration F, the coverage $c = 0.5$ makes the two Fe sites nonequivalent and, as a result, the Fe atom below oxygen moves outward the Fe layer, displacing therefore the O atoms of the interface TiO_2 layer in the same way. The structural distortions make the configuration F energetically unfavorable.

The energetics which is calculated for the coverage $c = 1$ can be explained using our findings for $c = 0.5$. We expect the two O adatoms occupy the positions above A and Ti. Here, P reversal gives a change in energy of about 0.2 eV for both systems. Any of the three other configurations TF, AF, or FF always includes at least one energetically unfavorable position atop Fe that drastically increases the associated surface energy. The configuration FF represents the most distorted system whose energy is larger by 12 eV (4 eV) compared to that of the AT configuration of PTO (BTO). For the same reason, the energetically favorable scenario of $c = 1.5$ is the configuration of ATF when one site above Fe is empty. Regarding $c = 2$, we have inspected two configurations: ATFF and 4H (shown in Fig. 1). It turns out that the 4H configuration, with all four hollow sites occupied by O, is unfavorable.

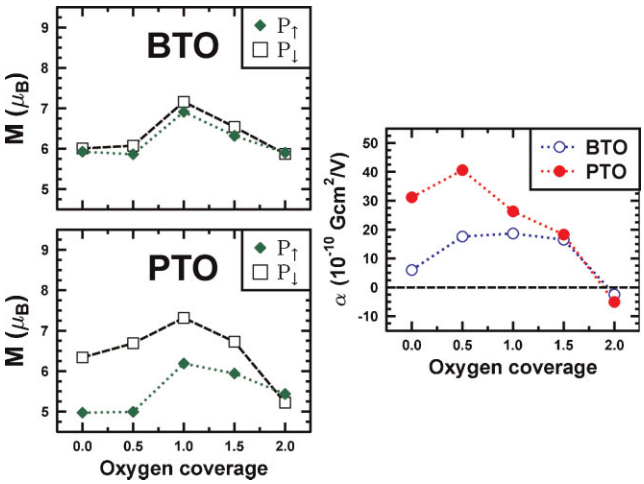

Figure 8 (online color at: www.pss-b.com) The total magnetization M of $O_x/Fe_2/ATO(001)$ (A = Ba, Pb, and $0 < x < 4$) as a function of oxygen coverage is shown in the two left panels. For each coverage the energetically favorable configuration was assumed. The estimated ME coupling coefficient α is shown in the right panel.

In the top panel of Fig. 8 we show the total M, calculated for the lowest-energy configuration of $O_x/Fe_2/ATiO_3$ for each O coverage. These are the configurations A, T, AT, ATF, and ATFF obtained for $c = 0.5$, 1, 1.5, and 2, respectively. For $c = 0.5$ we used the average between the A and the T configuration since they can coexist. The magnetization of uncovered Fe/PTO and Fe/BTO is also shown as well. The increase of M seen for $c = 0.5$ and 1, as compared to that of $c = 0$, is due to a induced magnetic moment at the O adatom which is aligned parallel to the Fe magnetic moment. In the case of low coverage, namely for $c = 0.5$ and 1, the Fe moment is not affected by the presence of adatoms. Contrarily, when the O adatom relaxes above Fe in the configurations ATF and ATFF, the Fe magnetic moment is decreased by about $1\mu_B$. This is mostly due to a relatively small distance between the O adatom and Fe along [001]. As a result, M gradually decreases with increasing $c > 1$.

It is obvious from Fig. 8 that in the case of O/Fe/BTO the magnitude of ΔM remains rather stable for O coverages $c < 1.5$. With further increase of c, $\Delta M \to 0$ at $c = 2$. For the PTO substrate, the trends of ΔM computed for $c > 1.5$ are similar to those of BTO. It should be kept in mind that the dense coverage of $c = 2$ is unrealistic since the highest oxidation state of iron seen in Fe_2O_3 mimics the coverage $c = 1.5$.

The right panel of Fig. 8 shows again the change of the interface ME coupling coefficient, α, which was evaluated like before as the ratio of the surface magnetization change $\mu_0 \Delta M/S$ and the coercive field E_c, where S is the interface area. The experimental $E_c = 10$ and 33 kV/cm were used for Fe/BTO and Fe/PTO, respectively. In general, the variation of α as a function of c follows the trends of ΔM. However, for $1 < c < 1.5$ we find that the two systems obey almost the same strength of α and, hence, there would be no advantage to use a highly polar PTO substrate for the dense O coverage.

3 Perspectives for future studies So far, the DFT studies of composite MF were focused on chemically perfect films and superlattices with no impurities. It is well known, however, that the magnetic order and related magnetic anisotropy of Fe films are very sensitive to the presence of some other 3d elements. The alloying effect may result in important changes in magnetoelectricity and therefore, the DFT-based modeling of chemical order in composite MF would be useful. For instance, our preliminary calculations of $(Fe_{2-y}Co_y)_L/BaTiO_3(001)$ performed with the use of the coherent-potential approximation to DFT demonstrate that the presence of Co above $y > 0.25$ at.% per each Fe atom may stabilize the FM order in the two ML thick and magnetically soft Fe films.

Another effect which leads to a large ME coupling at the biferroic interface, may come from magnetically ordered interfacial layer of the substrate. When BTO(001) is terminated by a CrO_2-ML instead of energetically preferable TiO_2 this enhances the ME coupling in Fe/BTO(001). Chromium dioxide is an experimentally proven half metal, which shows the Curie temperature of 392 K and which possesses the largest spin polarization reported for this class of materials. As a consequence of the half-metallic feature of CrO_2, the occupied Cr 3d bands are fully spin polarized, leading to the spin magnetic moment of $2\mu_B$ per formula unit. Regarding the Fe bilayer on CrO_2/BTO(001), we also expect the change of magnetic order under the P reversal.

There is one more prospective direction of the studies of composite MF, namely, the combination of the single-phase MF substrate and a strong ferromagnet. It has been already shown experimentally [30] that the exchange coupling between antiferromagnetic domains of $BiFeO_3$ and ferromagnetically ordered FeCo layer offers the possibility to vary the magnetization direction in FeCo by changing the polarization of $BiFeO_3$. Similarly, when the top FM layer of composite MF is replaced by a Co/Cu/Co multilayer, the interlayer exchange coupling must be accessible there. In Co/Cu/Co superlattice, the alignment of the magnetization direction in the Co layer, which can be either parallel or antiparallel, is determined by the thickness of Cu. The Co/Cu/Co/$BiFeO_3$ system and its ME coupling at the Co/$BiFeO_3$ interface, in principle, allow a P-induced switch of the interlayer exchange coupling. Here, the further investigations would be extremely important.

4 Summary In summary, the magnetism of composite MFs, realized by ultrathin Fe films on $ATiO_3$ perovskites (A = Ba, Pb, Sr), is found to exhibit a rich and peculiar structure, as is predicted from first-principles computational materials science. An FM-to-ferrimagnetic transition which is accompanied by a strong reduction of the Fe magnetic moments could be used in device applications to tailor the properties of the magnetic subsystem. Significant ME

coupling via the Fe/$ATiO_3$ interface is predicted, a spin-reorientation transition under switching is not found. In view of device applications it appears highly desirable to investigate theoretically and experimentally the thickness-dependent magnetic properties of Fe films sandwiched between ferroelectric perovskites.

Furthermore we discussed the effect of oxidation on the strength of ME coupling seen at the biferroic interface in epitaxial FM/ferroelectric nanocomposites. The oxygen coverage, ranging between $c = 0.5$ and two adsorbed O per Fe atom were simulated for $O_x/Fe_2/BaTiO_3(001)$ and $O_x/Fe_2/PbTiO_3(001)$ MFs. We suggest that oxygen adatoms may find their relaxed positions atop the Ba (Pb) and/or Ti sites. For $c > 1$, the magnetic properties computed for the Fe layer gradually degrade with increasing O coverage. However, when $c < 1.5$ the change in magnetization induced by polarization reversal is robust for all energetically preferable compositions. On the basis of our calculations we, therefore, suggest that intrinsic oxidation of biferroics may not destroy their magnetoelectricity significantly. In the case of realistic oxygen coverage ($c = 1$), we expect that the strength of ME coupling is similar for both biferroic systems under consideration.

Acknowledgements We thank D. Hesse for fruitful discussion. This work was supported by the *Sonderforschungsbereich* SFB 762, 'Functionality of Oxidic Interfaces'.

References

[1] K. F. Wang, J. M. Liu, and Z. F. Ren, Adv. Phys. **58**(4), 321–448 (2009).
[2] H. Schmid, J. Phys.: Condens. Matter **20**(43), 434201 (2008).
[3] W. Eerenstein, M. Wiora, J. L. Prieto, J. F. Scott, and N. D. Mathur, Nature Mater. **6**, 348–351 (2007).
[4] S.-W. Cheong, Nature Mater. **6**, 927–928 (2007).
[5] F. Zavaliche, T. Zhao, H. Zheng, F. Straub, M. P. Cruz, P.-L. Yang, D. Hao, and R. Ramesh, Nano Lett. **7**(6), 1586–1590 (2007).
[6] G. A. Smolenskii and I. E. Chupis, Sov. Phys. Usp. **25**, 475 (1982).
[7] M. Dawber, K. M. Rabe, and J. F. Scott, Rev. Mod. Phys. **77**, 1083–1130 (2005).
[8] D. Khomskii, Physics **2**(20), 1–8 (2009).
[9] M. Fiebig, J. Phys. D, Appl. Phys. **38**(8), R123–R152 (2005).
[10] S. Picozzi and C. Ederer, J. Phys.: Condens. Matter **21**(30), 303201 (2009).
[11] J. M. Rondinelli, M. Stengel, and N. A. Spaldin, Nature Nanotechnol. **3**, 46–50 (2008).
[12] C.-G. Duan, S. S. Jaswal, and E. Y. Tsymbal, Phys. Rev. Lett. **97**, 047201 (2006).
[13] M. Fechner, I. V. Maznichenko, S. Ostanin, A. Ernst, J. Henk, P. Bruno, and I. Mertig, Phys. Rev. B **78**(21), 212406 (2008).
[14] C. Yu, M. J. Pechan, S. Srivastava, C. J. Palmstrom, M. Biegaslski, C. Brooks, and D. Schlom, J. Appl. Phys. **103**(7), 07B108 (2008).
[15] C.-G. Duan, J. P. Velev, R. F. Sabirianov, W. N. Mei, S. S. Jaswal, and E. Y. Tsymbal, Appl. Phys. Lett. **92**(12), 122905 (2008).
[16] M. K. Niranjan, J. P. Velev, C.-G. Duan, S. S. Jaswal, and E. Y. Tsymbal, Phys. Rev. B **78**(10), 8 (2008).
[17] C. A. F. Vaz, J. Hoffman, A.-B. Posadas, and C. H. Ahn, Appl. Phys. Lett. **94**(2), 022504 (2009).
[18] C. Israel, N. D. Mathur, and J. F. Scott, Nature Mater. **7**(2), 93–94 (2008).
[19] G. Kresse and J. Furthmüller, Phys. Rev. B **54**, 11169–11186 (1996).
[20] M. Luders, A. Ernst, W. M. Temmerman, Z. Szotek, and P. J. Durham, J. Phys.: Condens. Matter **13**(38), 8587–8606 (2001).
[21] J. Henk, H. Mirhosseini, P. Bose, K. Saha, N. Fomynikh, T. Scheunemann, S. V. Halilov, E. Tamura, and R. Feder, OMNI – Fully relativistic electron spectroscopy calculations, 2008. The computer code is available from the authors.
[22] M. Fechner, S. Ostanin, and I. Mertig, Phys. Rev. B **77**(9), 094112 (2008).
[23] J. Henk, A. M. N. Niklasson, and B. Johansson, Phys. Rev. B **59**(14), 9332–9341 (1999).
[24] S. Ostanin, S. S. A. Razee, J. B. Staunton, B. Ginatempo, and E. Bruno, J. Appl. Phys. **93**(1), 453–457 (2003).
[25] J. B. Staunton, S. Ostanin, S. S. A. Razee, B. L. Gyorffy, L. Szunyogh, B. Ginatempo, and E. Bruno, Phys. Rev. Lett. **93**(25), 257204 (2004).
[26] T. C. Leung, C. T. Chan, and B. N. Harmon, Phys. Rev. B **44**(7), 2923–2927 (1991).
[27] M. Fechner, S. Ostanin, and I. Mertig, Phys. Rev. B **80**(9), 094405 (2009).
[28] H. J. Monkhorst and J. D. Pack, Phys. Rev. B **13**, 5188–5192 (1976).
[29] R. Q. Wu and A. J. Freeman, J. Magn. Magn. Mater. **127**(3), 327–345 (1993).
[30] Y.-H. Chu, L. W. Martin, M. B. Holcomb, M. Gajek, S.-J. Han, Q. He, N. Balke, C.-H. Yang, D. Lee, W. Hu, Q. Zhan, P.-L. Yang, A. Fraile-Rodriguez, A. Scholl, S. X. Wang, and R. Ramesh, Nature Mater. **7**(6), 478–482 (2008).